Multielectron effect in the strong-field ionization of aligned nonpolar molecules

M. Abu-samha◉

College of Engineering and Technology, American University of the Middle East, Egaila 54200, Kuwait

Lars Bojer Madsen◉

Department of Physics and Astronomy, Aarhus University, 8000 Aarhus C, Denmark

We revisit strong-field ionization of aligned O_2, CO_2, and CS_2 molecules in light of recent advances in the field of strong-field physics, in particular the inclusion of multielectron polarization in the numerical solution of the time-dependent Schrödinger equation (TDSE) within the singe-active-electron approximation. Multielectron polarization is modeled by the introduction of a long-range induced dipole term based on the polarizability of the cation, and a field at short distances that counteracts the applied external field and leads to a vanishing time-dependent interaction within a certain cutoff radius. For the probed molecules, the main effect of including multielectron polarization is the reduction of the total ionization yields (TIYs), and for molecules with large polarizability of their cation (CO_2 and CS_2), the alignment angle of maximum TIY will shift. The photoelectron momentum distributions and above-threshold ionization spectra show little imprint of the multielectron polarization associated with the long-range part of the laser-induced dipole potential. For CO_2 and CS_2, the inclusion of multielectron polarization and the associated induced dipole potential in the TDSE model gives alignment-resolved distributions of total ionization yields which are in better agreement with the available experimental results.

I. INTRODUCTION

In strong-field ionization of atomic and molecular targets by intense laser pulses, the time-dependent Schrödinger equation (TDSE) is often used within the single-active-electron (SAE) approximation to describe the ionization process. In this approach, the SAE orbital is propagated in the combined potential of the atom or molecule and the external field. SAE potentials have been successfully applied for some atoms [1,2] and molecules [3–6].

While the performance of the SAE approximation is generally accepted, some cases where account of multielectron effects are needed have been discussed in the literature including, for example, the CO [7,8] and OCS [9] molecules. For these molecules, the calculated ionization yields and their orientation dependence are affected by multielectron polarization (MEP) or some artifacts of solving the TDSE within the SAE approximation such as the shifting of population from the highest occupied molecular orbital (HOMO) to lower-lying orbitals of the potential. The latter observation was recently illustrated for CO in Ref. [8]: the dipole matrix elements which couple the HOMO to lower-lying orbitals are strongly dependent on molecular orientation, and the total ionization yields (TIYs) calculated at different orientation angles are strongly affected by such dipole transitions and the associated artificial shifting of population. As a consequence, for CO, solving the TDSE within the SAE approximation without accounting for MEP predicts the wrong orientation dependence of the TIYs [8]: the TDSE results predict a maximum TIY at the orientation angle $\beta = 180°$, that is, when the maximum of the electric field points from the O-end to the C-end, which is contrary to experimental observations [10]. The performance of the TDSE method for CO was significantly improved upon inclusion of MEP [8]. Indeed, by extending the TDSE method with a MEP treatment following the approach of Refs. [11,12], the inclusion of MEP within the SAE model results in negligible dipole coupling of the HOMO to lower-lying orbitals and the predicted angular distribution of TIYs is in good agreement with the experimental [10] and theoretical [11,13] data. In this connection, we also note that inclusion of MEP recently led to improved agreement between theory and experiment for odd-even high harmonic generation in CO [14].

In the case of CO, the long-range correction term of the induced dipole potential was not needed to produce the correct trend in TIYs for the CO molecule. It is sufficient to simply turn off the laser interaction within a certain molecular cutoff radius, r_c. The effective turning off of the molecule-laser interaction for $r < r_c$ is a consequence of the polarization of the remaining electrons. The electric field associated with this polarization counteracts the applied external field and leads to a cancellation of the interaction. In this sense, the cancellation is a result of the rearrangement of the remaining electrons until they feel no effective field, i.e., a rearrangement that leads to a field inside r_c that has a direction opposite to the applied field, but with the same magnitude. We will come back to this effect and the value of r_c below.
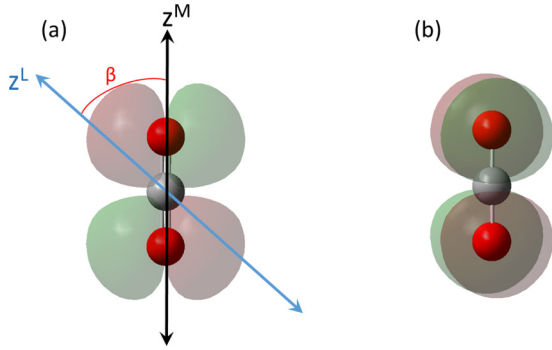
FIG. 1. Illustration of the degenerate HOMOs of π symmetry in CO_2 in the molecular fixed (superscript M) (a) $(xz)^M$ and (b) $(yz)^M$ planes. In (a), the laboratory-frame z^L axis and alignment angle (β) are illustrated. The HOMO(yz) in (b) always has a node in the polarization direction. This is not the case with the HOMO (xz) in (a).

For OCS, experimental measurements of TIYs and their orientation dependence have attracted much attention in the recent literature [15–19] due to discrepancies between experimental observations and theoretical predictions. In Ref. [17], the experiments were conducted using linearly polarized laser pulses with 30-fs duration at an 800-nm wavelength and intensities of 1.5×10^{14} and 1.8×10^{14} W/cm^2. At these conditions, the TIY was measured as a function of the orientation angle, and a minimum TIY was obtained at laser polarization parallel to the molecular axis ($\beta = 0°$), whereas the maximum TIY was obtained at laser polarization perpendicular to the molecular axis ($\beta = 90°$). The orientation dependence of the TIYs presents a challenge to ionization models. For the OCS molecule, the molecular Ammosov-Delone-Krainov model [20] and the strong-field approximation (SFA) [21–23] predict the angular dependence of TIYs to follow the orbital structure. In these models, the maximum TIY is predicted at β close to 35°. Also the Stark-corrected molecular tunneling theory [24,25] and the weak-field asymptotic theory of tunneling, which includes dipole effects [26,27], did not reproduce the experimental results for the OCS molecule [28]. In Ref. [9], we presented theoretical calculations of orientation-dependent TIYs from the HOMO of OCS in a strong linearly polarized laser field by solving the TDSE within the SAE approximation and including MEP effects. The MEP term was represented by an induced dipole term which contains the polarizability of the OCS$^+$ cation parallel to the laser polarization. After adequately accounting for the laser-induced dipole potential associated with the MEP term, the calculated TIYs and their orientation dependence are in good agreement with the experimental measurements reported in Ref. [17]. The results indicated that the polarizability anisotropy of OCS$^+$ was primarily responsible for the orientation dependence of TIYs from the HOMO of OCS.

In this paper, we study strong-field ionization of aligned nonpolar molecular targets: O_2, CO_2, and CS_2. The HOMOs of these molecules have π_g symmetry; see the degenerate HOMOs of CO_2 in Fig. 1, and the ionization potentials are comparable; for the ionization potentials, we use the negative of the HOMO energies listed in Table I. The HOMO(yz) in

TABLE I. HOMO energies (E_{HOMO}) and molecular-fixed frame polarizability components (α_{xx}, α_{zz}) of the O_2^+, CO_2^+, and CS_2^+ cations as obtained from quantum chemistry calculations at the B3LYP level of theory (MP2 for CO_2^+ polarizability). All quantities are in atomic units.

	E_{HOMO}	α_{xx}	α_{zz}
O_2^+	−0.3199	5.08	9.41
CO_2^+	−0.3845	7.29	30.42
CS_2^+	−0.2805	28.32	76.77

Fig. 1(b) has a node in the polarization direction; it is therefore expected that its contribution to ionization is negligible compared to that of the HOMO(xz) in Fig. 1(a).

For CO_2, experimental measurements [29] revealed a narrow angular distribution of TIYs with a maximum TIY at alignment angle $\beta = 45°$. For CS_2, the experimental data [30] are consistent with those for CO_2 in that an alignment angle of $\beta = 45°$ provides the largest ionization yield. Moreover, the CS_2 measurements revealed sharp radial structures in the photoelectron momentum distributions (PMDs) of aligned CS_2, an effect that was attributed to Rydberg states brought into resonance by the ac Stark shift [30].

In our earlier work on CO_2 [31], strong-field ionization from the HOMO of CO_2 was modeled by SAE-TDSE calculations without accounting for MEP, and although our TDSE calculations predicted the correct alignment angle of the TIYs, the calculations suffered from shifting of population into lower-lying orbitals. Here, we revisit strong-field ionization of CO_2 in light of the recent advances in the treatment of MEP within the SAE approximation. The questions we address here are whether the TDSE results for O_2, CO_2, and CS_2 can be improved simply by turning off the external field within r_c, thereby minimizing the shifting of population to lower-bound states, or whether the long-range part of the MEP term, represented by a field-induced dipole term, which depends on the polarizability of the cations (see Table I and discussion below), has an effect on the angular distributions of the TIYs and PMDs. To address these questions, TDSE calculations were conducted using linearly polarized laser pulses with different laser peak intensities and pulse durations. First, we show how the SAE-TDSE performance is improved once the external field is turned off within r_c; we use the CO_2 as a proof-of-principle case. Then, we discuss the effects of long-range MEP on the alignment dependence of TIYs and PMDs for O_2, CO_2, and CS_2.

The theoretical and computational models are presented in Sec. II, followed by results and discussion in Sec. III and conclusions in Sec. IV. Atomic units are used throughout, unless otherwise stated.

II. THEORETICAL MODELS

The SAE potentials describing O_2, CO_2, and CS_2 were determined from quantum chemistry calculations [32], following the procedure detailed in Ref. [3]. For O_2 and CO_2, the HOMO was obtained in TDSE calculations by propagation in imaginary time. For CS_2, the HOMO was obtained following the procedure laid out in Ref. [8].

In our TDSE method, the time-dependent wave function $\psi(\vec{r}, t)$ of the active orbital is represented by a partial wave expansion in which the spherical harmonics $Y_{lm}(\Omega)$ are used to describe the angular degrees of freedom and a radial grid is used for the time-dependent reduced radial waves, $f_{lm}(r, t)$, i.e.,

$$\psi(\vec{r}, t) = \sum_{lm} \frac{f_{lm}(r, t)}{r} Y_{lm}(\Omega). \qquad (1)$$

The TDSE is solved for an effective one-electron potential describing the interaction with the nucleus, the remaining electrons, and the external field. The TDSE is propagated in the length gauge (LG) [33] with a combined split-operator [34] Crank-Nicolson method. The electric field $E(t)$, linearly polarized along the laboratory-frame z axis (from now on the superscript "L" denoting the laboratory-fixed frame is skipped for brevity), is defined in terms of the vector potential $A(t)$ by

$$\vec{E}(t) = -\partial_t \vec{A}(t) = -\partial_t \left[\frac{E_0}{\omega} \sin^2(\pi t / \tau) \cos(\omega t + \phi) \right] \hat{z}, \quad (2)$$

where E_0 is the field amplitude, ω the angular frequency, and ϕ the carrier-envelope phase (CEP) for a laser pulse with duration τ. We use a frequency of $\omega = 0.057$ a.u., corresponding to a wavelength of 800 nm. The CEP is kept fixed ($\phi = -\pi/2$). The radial grid contains up to 4096 points and extends to 320 a.u. For the listed molecules, the size of the angular basis set is limited by setting $l_{\max} = 30$ ($l_{\max} = 40$ for convergence tests) in Eq. (1).

The above-threshold ionization (ATI) spectra and PMDs in the polarization plane, dP/dk_{xz}, were produced by projecting $\psi(\vec{r}, t = \tau)$ at the end of the laser pulse on scattering states of the Coulomb potential in the asymptotic region, and the TIYs were obtained by integrating the ATI spectra. This approach was recently implemented successfully to obtain TIYs from oriented CO [8] and OCS [9]. In all the PMDs presented in Sec. III, the signal at momenta below 0.1 a.u. is removed from the PMDs: we find very high yields at low momenta and keeping this inner part of the signal would prevent the resolution of the features in the PMD that we wish to discuss.

A. Extending TDSE methodology with multielectron polarization

The theory for the effect of MEP on strong-field ionization was developed in Refs. [24,25,35,36]. For the nonpolar molecules addressed here, in the case when MEP is taken into consideration, the effective potential describing the interaction of the active electron with the core and the time-dependent external field is given asymptotically at large distances as

$$V_{\text{eff}}(\vec{r}, t) = \vec{r} \cdot \vec{E}(t) - \frac{1}{r} - \frac{\vec{\mu}_{\text{ind}} \cdot \vec{r}}{r^3} \cdots, \qquad (3)$$

where $\vec{\mu}_{\text{ind}}$ is the induced dipole of the cation. Notice that the SAE potential used in most TDSE calculations is missing the induced dipole potential, $-\vec{\mu}_{\text{ind}} \cdot \vec{r}/r^3$. The MEP term is expressed as $-\vec{\mu}_{\text{ind}} \cdot \vec{r}/r^3 = -[\boldsymbol{\alpha} \cdot \vec{E}(t)] \cdot \vec{r}/r^3$, where $\boldsymbol{\alpha}$ denotes the polarizability tensor. For the linear molecules considered here, and a linearly polarized field with polarization along the z direction, the product $\boldsymbol{\alpha} \cdot \vec{E}(t)$ simplifies to $(\alpha_\perp E_z, 0, \alpha_{||} E_z)$. In the laboratory frame, the components perpendicular ($\alpha_\perp$)

and parallel ($\alpha_{||}$) to the laser polarization can be obtained from the molecular-fixed frame components α_{xx} and α_{zz} in Table I by a simple rotation:

$$\alpha_\perp = (\alpha_{zz} - \alpha_{xx}) \sin(\beta) \cos(\beta), \qquad (4)$$

$$\alpha_{||} = \alpha_{xx} \sin^2(\beta) + \alpha_{zz} \cos^2(\beta). \qquad (5)$$

At alignment angles $\beta = 0°$ or $90°$, $\alpha_\perp$ and the corresponding induced dipole component vanish. At other alignment angles, however, there is a nonvanishing contribution to the induced dipole from $\alpha_\perp$. We have checked for the molecules considered here that the induced dipole component from $\alpha_\perp$ can be omitted: For CO_2 (CS_2) at $\beta = 45°$ within a static external field $E_z = -0.035$ a.u., the laboratory-fixed frame induced dipole components are $\mu_{\text{ind},x} = 0.59$ (2.60) and $\mu_{\text{ind},z} = -1.71$ (-6.15) Debye, as obtained from quantum chemistry calculations in GAMESS [32]. For the O_2 molecule at alignment angle $\beta = 45°$ and at the same external field strength as for CO_2 and CS_2, the induced dipole components are quite small ($\mu_{\text{ind},x} = 0.35$ and $\mu_{\text{ind},z} = -1.1$ Debye) since the polarizability components are small; see Table I. For the considered molecules, the contribution to the induced dipole from $\alpha_\perp$ will be neglected in the present work. This approach was recently applied successfully to strong-field ionization of CO [8] and OCS [9] with theoretical results in agreement with the experimental data.

Based on the preceding discussion, the MEP term is approximated as $-\vec{\mu}_{\text{ind}} \cdot \vec{r}/r^3 \approx -\alpha_{||} \vec{E}(t) \cdot \vec{r}/r^3$, where $\alpha_{||}$ is the static polarizability of the cation parallel to the laser polarization axis. A cutoff radius is chosen close to the core at a radial distance

$$r_c = \alpha_{||}^{1/3}, \qquad (6)$$

such that the MEP cancels the external field at $r \leqslant r_c$ [12,35,36]. The interaction term including MEP correction is expressed in the LG at each radial grid point r_i as

$$V_{\text{LG}}^{\text{Ext}}(r_i, t) = \begin{cases} \left(1 - \frac{\alpha_{||}}{r_i^3}\right) E(t) \sqrt{\frac{2}{3}} r_i \bar{P}_1(\zeta), & r > r_c \\ 0, & r \leqslant r_c, \end{cases} \qquad (7)$$

where $E(t)$ is the electric field at time t, $\bar{P}_1$ is a normalized Legendre function, and $\zeta = \cos(\theta)$ where θ is the polar angle of the electron coordinate $\vec{r}$. Based on the above equation, one can see that MEP results in two related effects: the electrons in the cation polarize and set up a field that counteracts the externally applied field at short distances. Hence, the interaction between the single-active electron and the laser field is effectively turned off at $r \leqslant r_c$ [35,36]. At long range, that is at $r > r_c$, the MEP is represented by an induced dipole potential with a magnitude that depends on the external field strength and the polarizability of the cation.

The polarizability components for the O_2^+, CO_2^+, and CS_2^+ cations were obtained from the NIST computational chemistry database (CCCBDB) [37]; see Table I. The quantum chemistry calculations of molecular polarizability were conducted at the B3LYP (MP2 for CO_2^+) level of theory.
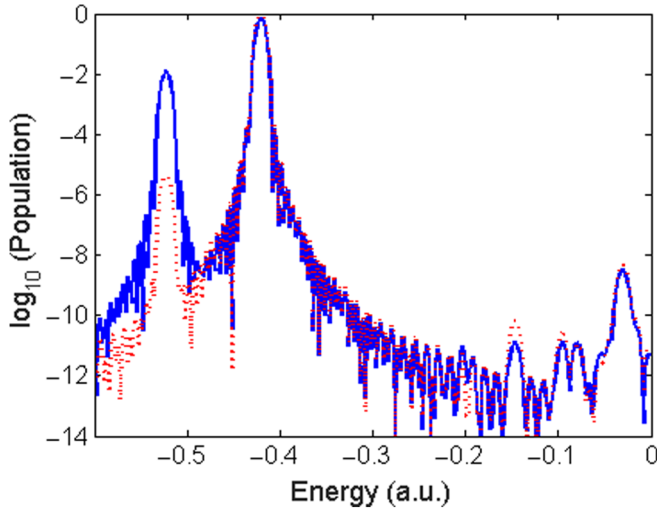
FIG. 2. Bound state spectrum of CO_2 after the end of an 800-nm laser pulse containing five optical cycles with peak intensity of 5.6×10^{13} W/cm^2. The solid (dotted) line denotes TDSE calculations without (with) MEP correction.

III. RESULTS AND DISCUSSION

A. Improving the single-active-electron approximation for CO_2

Our earlier TDSE calculations for CO [38] and CO_2 [31] within the SAE approximation suffered from shifting of the population to lower-lying orbitals of the potential, as was recently discussed for CO in Ref. [8]. The problem is illustrated for CO_2 in Fig. 2 (solid line). In this figure, the bound state spectrum is produced for CO_2 after probing the molecule by a five-cycle laser pulse with an intensity of 5.6×10^{13} W/cm^2 and $\omega = 0.057$ a.u. In Fig. 2, the peaks at ~ -0.4 a.u. and -0.55 a.u. correspond to the (Π_g) HOMO (see Fig. 1) and HOMO-1 of CO_2. In the present approach, we consider only the HOMO as being active and it should not populate the HOMO-1 since the latter orbital is already occupied.

Here, we consider an improved theory for calculating the TIYs from aligned CO_2 which takes into account the MEP effect and, thereby, resulting in minimized shifting of the population from the HOMO to the lower-lying occupied orbitals of the potential. This is accomplished by turning off the external field within r_c of Eq. (6), such that the MEP cancels the external field at $r \leqslant r_c$ [12,35,36]. The improvement of the SAE approximation following the implementation of this effect is illustrated in Fig. 2 (dotted line). Here it can be seen that the population in the HOMO-1 (at energy -0.55 a.u.) is reduced by 3–4 orders of magnitude. Meanwhile, the population in the excited states is less sensitive to turning the external field off within the cutoff radius r_c. The effective turning off of the external field within the radius r_c means that there is very little coupling to states that are mainly localized within that radius. This is the reason why the coupling to the lower, localized states is decreased substantially, while the coupling to the excited states (which are more diffuse) is affected to a lesser extent. This is promising in particular for cases where strong-field ionization is affected by the excited-state manifold. The preceding results and discussion show that

it is necessary to turn off the external field within r_c in all TDSE calculations within the SAE approximation.

B. Effect of long-range multielectron polarization on alignment-dependent total ionization yields and photoelectron momentum distributions of CO_2

Now we discuss, in addition to turning off the time-dependent interaction below r_c, the effect of accounting for the long-range MEP correction in TDSE calculations on the calculated TIYs from the degenerate HOMOs of aligned CO_2 (shown in Fig. 1). The probe laser pulses contain five optical cycles, a wavelength of 800 nm, and peak laser intensities of 1.4×10^{13}, 3.2×10^{13}, 5.6×10^{13}, and 8.8×10^{13} W/cm^2. The effect of the long-range MEP correction on angular distributions of TIYs is shown in Fig. 3. The TIYs presented in Fig. 3 are incoherent sums of the ionization yields from the HOMO(xz) and HOMO(yz) of CO_2. The TIYs were calculated by integrating the ATI spectra produced by projecting the wave packet at the end of the laser pulse on Coulomb scattering states in the asymptotic region; see Sec. II and Refs. [8,9,39].

We judge the quality of the theoretical TIYs for aligned CO_2 based on the following two criteria: the alignment angle of maximum TIY and the ratio of TIYs at alignment angles $\beta = 45°$ and $0°$. Based on early experimental measurements on CO_2 [29], the alignment angle of maximum TIY should be $\beta = 45°$ and the ratio TIY($\beta = 0°$)/TIY($\beta = 45°$) is approaching zero. In Fig. 3, we compare the angular distributions of TIYs for CO_2 obtained from TDSE calculations with and without accounting for long-range MEP correction, implemented in Eq. (7). Notice that in both cases, the field is turned off within r_c, as we have established based on the results of Sec. III A.

From the TDSE calculations for CO_2 at the relatively lower intensities of 1.4×10^{13} and 3.2×10^{13} W/cm^2 [see Figs. 3(a) and 3(b)], it is evident that although the maximum ionization yield is predicted correctly simply by turning off the external field within r_c, the alignment dependence of the TIY seems to be correctly described only when the full MEP term, including the long-range induced dipole potential, is accounted for. The effect of including long-range MEP seems to decrease the relative ionization probability at $\beta = 30°$. For CO_2 at the higher intensities of 5.6×10^{13} and 8.8×10^{13} W/cm^2 [see Figs. 3(c) and 3(d)], the full MEP term, including the long-range induced dipole potential, should be accounted for in order to correctly predict the alignment angle of the maximum TIY. Regarding the ratio of TIYs, i.e., TIY($\beta = 0°$)/TIY($\beta = 45°$), we note that while the experimental results predict that this ratio should approach zero [29], it seems that the MEP-corrected TDSE calculations presented here and in Ref. [11] overestimate the ratio of TIYs at the higher intensities. On a positive note, based on Fig. 3, the ratio TIY($\beta = 0°$)/TIY($\beta = 45°$) is smaller when the long-range MEP term is accounted for. In this sense, accounting for MEP seems to reduce the gap between the theory and experiment.

Notice that for CO_2, the TIYs presented in Fig. 3 are incoherent sums of the contributions of the ionization yields from the HOMO(xz) and HOMO(yz); see the sketch of HOMOs in Fig. 1. To explore the effect of including MEP on these
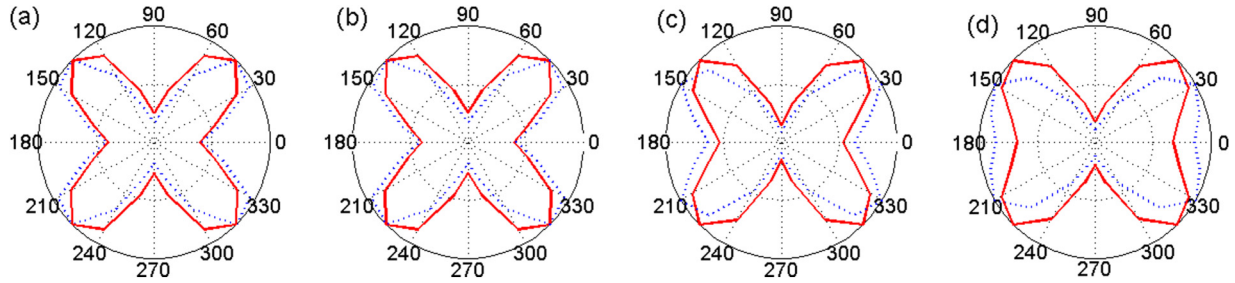
FIG. 3. Effect of MEP on the alignment dependence of TIYs from the HOMOs of the CO_2 molecule at peak intensities of (a) 1.4×10^{13}, (b) 3.2×10^{13}, (c) 5.6×10^{13}, and (d) 8.8×10^{13} W/cm^2. The dotted lines denote no field within r_c, while the solid lines denote full MEP including the long-range laser-induced dipole potential.

orbitals, we show separate angular distributions of ionization yields from HOMO(xz) and HOMO(yz) in Fig. 4. Notice that at an alignment angle $\beta = 0°$, the HOMO(xz) and HOMO(yz) orbitals give the same ionization yields. In Fig. 4, however, the TIYs in each panel are normalized to unity in order to clearly display the effect of including MEP. As can be seen from Fig. 4 at high intensities, while the effect of including MEP is very significant for the HOMO(xz), it has little effect on the angular distributions of ionization yield from the HOMO(yz). We also note that the angular distributions of ionization yields from the HOMO(xz) closely resemble the summed-up TIYs shown in Fig. 3, which is as expected since the HOMO(yz) has a node in the polarization direction and therefore contributes less to the TIYs. In the following, the results on angle-resolved TIYs show the yields incoherently summed over the contributions from the two orbitals. In all cases, the contribution from the HOMO(xz) orbitals dominates.

Next, we discuss the connection between the MEP effect and pulse length, for TDSE calculations at a laser intensity of 8.8×10^{13} W/cm^2. To this end, alignment-dependent TIYs were calculated for CO_2 probed by laser pulses containing two, five, and eight optical cycles, and the results are shown in Fig. 5. For all considered pulse lengths, the alignment angle of maximum TIY shifts from 30° (when the long-range MEP term is omitted) to 45° (when full MEP is accounted for), indicating that this characteristic result is insensitive to

pulse length. In short, taking MEP into account improves the prediction of alignment angle (β) of the maximum TIY, in comparison with the experimental measurements, in particular at high laser intensities.

To shed some light on the physics underlying the results in Fig. 3, in particular the effect of long-range MEP on the angular distributions of TIYs, we refer to tunneling theory. It is well known that for electron tunneling through a potential barrier, the tunneling rate decreases as the height or width of the barrier increases. In our TDSE model, the long-range effect of MEP is represented by an induced dipole term based on the polarizability of the cation; see Eq. (7). From plots of the field-dressed SAE potential for CO_2 at an alignment angle $\beta = 0°$ (see Fig. 6), we conclude that including the long-range MEP will increase the height of the tunneling barrier and therefore reduce the ionization yield. This explains why the ionization yield is suppressed when the MEP term is accounted for. This effect becomes more pronounced as the laser intensity increases; cf. Figs. 6(a) and 6(b). We have also calculated the tunneling exit points for CO_2 at orientation angles $\beta = 30°$ and 45° based on Eq. (15) in Ref. [40]. At a field strength (of 0.04 a.u.) corresponding to a laser intensity of 5.6×10^{13} W/cm^2, the tunneling exit points at $\beta = 30°$ and 45°, respectively, are −9.34 a.u. (−9.32 a.u. without MEP) and −9.38 a.u. (−9.36 a.u. without MEP). Hence the difference in the tunneling exit at $\beta = 30°$ and 45° is relatively
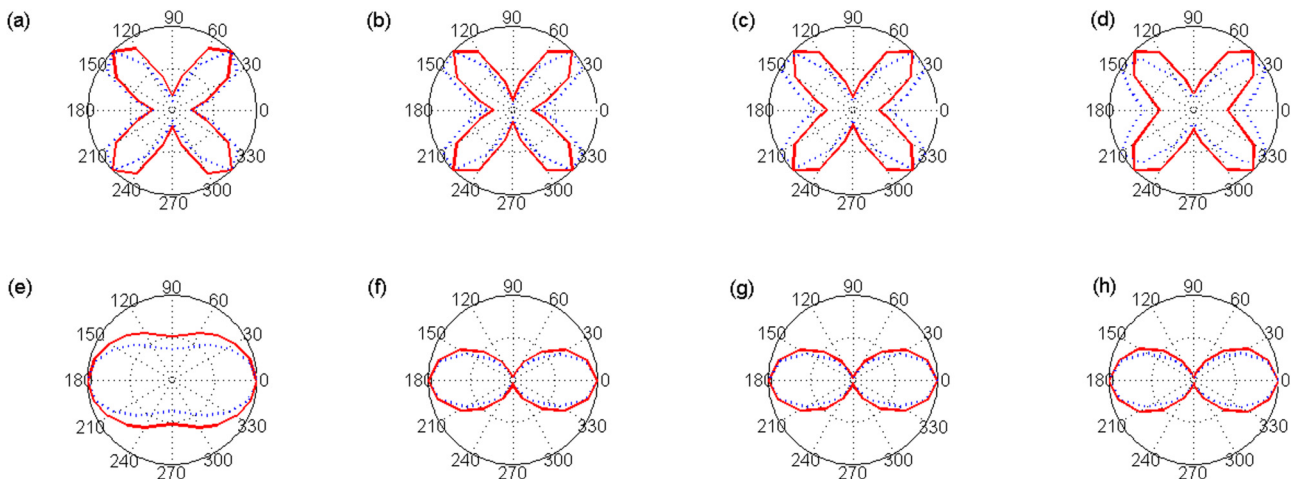

FIG. 4. Contributions from the (a)–(d) HOMO(xz) and (e)–(h) HOMO(yz) of CO_2 to the TIYs shown in Fig. 3. In each panel, the TIYs are normalized to unity.
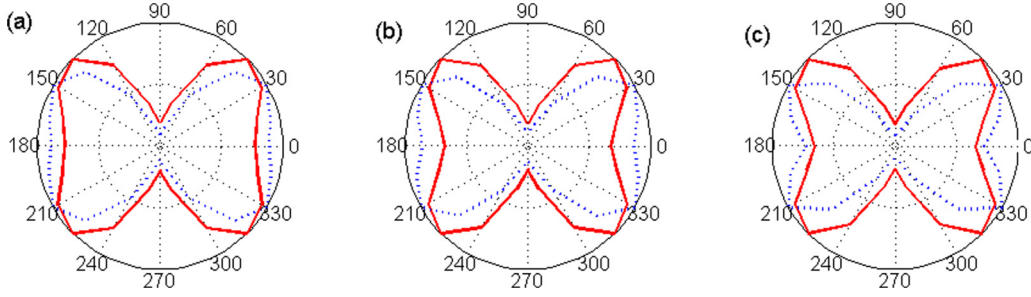
FIG. 5. Effect of MEP on the alignment dependence of TIYs from the HOMOs of the CO_2 molecule at peak intensity of 8.8×10^{13} W/cm^2 for pulses containing (a) two, (b) five, and (c) eight optical cycles. The dotted lines denote no field within r_c, while the solid lines denote full MEP including the long-range laser-induced dipole potential.

small and insensitive to the MEP correction. We can therefore explain the change in TIYs based on the change in tunneling barrier height. To be more precise, we can explain the shift of the ionization peak from $\beta = 30°$ to $45°$ based on the parallel polarizabilities (and corresponding r_c values) for CO_2^+ at $\beta = 30°$ and $45°$ as follows: at $\beta = 30°$ ($45°$), $\alpha_{\parallel} = 26.1375$ a.u. (20.355 a.u.) and $r_c = 2.968$ a.u. (2.730 a.u.). Based on these numbers, it can clearly be seen that the polarizability at $\beta = 30°$ is larger than at $45°$, meaning a higher tunneling barrier and therefore more suppression of TIYs.

Recently, the effect of including MEP on alignment-dependent TIYs from the HOMO of CO_2 was investigated by a TDSE method in Ref. [11]. Based on their results for CO_2 (cf. Fig. 6(c) of Ref. [11]), the alignment angle of the maximum TIY ($\beta = 45°$) is not sensitive to the inclusion of MEP in the TDSE treatment. This is in surprising contrast to the results presented here. According to Ref. [11], the TIY for CO_2 at alignment angle $\beta = 0°$ should increase upon inclusion of MEP, which is rather contrary to the common understanding of the MEP effect based on Eq. (7) and the behavior of the field-dressed potential as shown in the plots of the field-dressed SAE potential for CO_2 in Fig. 6: inclusion of the induced dipole term increases the height of the tunneling barrier and therefore reduces the ionization yield compared to the case without inclusion of MEP. Notice that for CO_2, the polarizability of the cation is largest at $\beta = 0°$ ($\alpha_{\parallel} = 30.42$ a.u.), which suggests that inclusion of MEP should result in a significant suppression (not enhancement) of the TIY at $\beta = 0°$. We

also notice that the calculations in Ref. [11] were conducted at a laser intensity (of 2×10^{14} W/cm^2) which is well above the over-barrier intensity (OBI) for CO_2, as can be seen from the sketch of the field-dressed potential for CO_2 in Fig. 6(b), whereas we consider laser intensities up to 8.3×10^{13} W/cm^2. In our approach, we represent MEP in the length gauge (see Sec. II) and we found that the convergence of TDSE calculations becomes more challenging at higher intensities.

Now that we have addressed the effect of MEP on the angular distributions of TIYs, we consider the question of whether such an effect can be observed experimentally. Since a full intensity averaging is unfortunately beyond the reach of the present TDSE approach due to its high computational cost, we have performed convolution of single-intensity theoretical distributions of TIYs, taken from Fig. 3(d), with the experimental convolution function given in Ref. [29]. The results are shown in Fig. 7. Here, Fig. 7(a) shows the data from Fig. 3(d), but interpolated to a denser grid in alignment angle. In Fig. 7(b), we then show the result of convoluting the data in Fig. 7(a) by the function used in the experiment. From Fig. 7(b), one can see that the convolution procedure smooths the angular variation, such that although the peak position shifts by $15°$, the convoluted data only change slightly. This means that an analysis of MEP based solely on experimental results will be challenging unless the MEP-induced change in alignment angle is large.
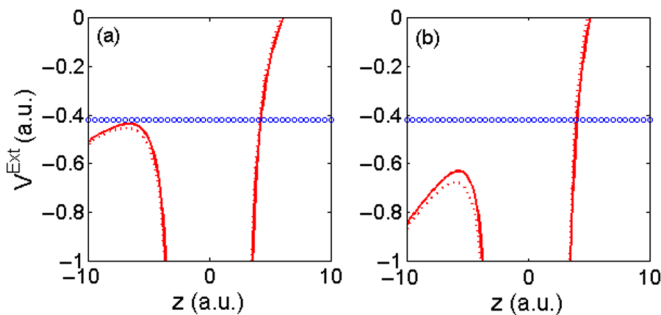

FIG. 6. Field-dressed SAE potential for CO_2 along the molecular axis ($\beta = 0°$) at external field strength values (a) $E = 0.04$ a.u. and (b) $E = 0.075$ a.u. In (a) and (b), solid lines denote full MEP; dotted lines: no MEP; blue circles: field-free ionization potential.
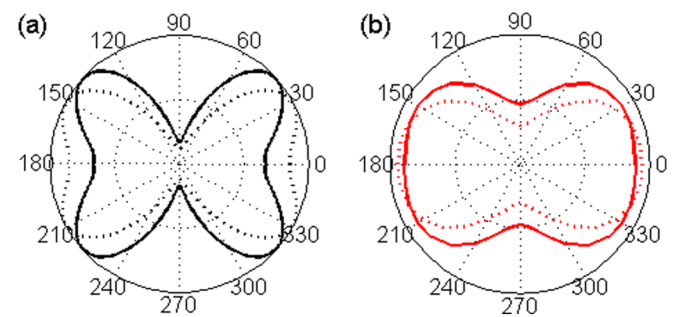

FIG. 7. (a) Interpolation of the theoretical distributions of TIYs from CO_2 presented in Fig. 3(d) in order to obtain an estimate for the TIYs at a denser angular grid. In (b), the theoretical yields in (a) were convoluted with an experimental convolution function taken from Ref. [29]. Solid lines denote full MEP; dotted lines: no field within r_c.
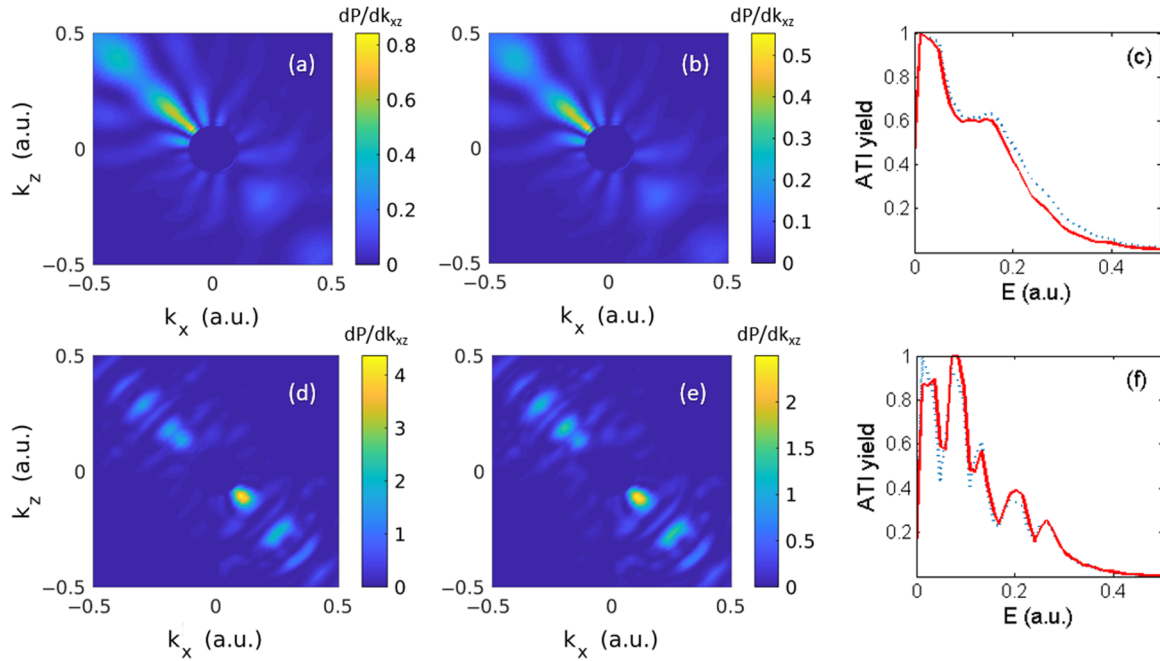
FIG. 8. Effect of MEP on laboratory-frame PMDs and ATI spectra from the HOMO(xz) of the CO_2 molecule at a peak intensity of 8.8×10^{13} W/cm^2 and alignment angle $\beta = 45°$ for 800 nm pulses containing (a)–(c) two and (d)–(f) eight cycles. The PMDs in (a), (d) refer to TDSE calculations with no field within r_c, while (b), (e) refer to the full MEP account. In the ATI spectra in (c), (f), the dotted lines (solid lines) denote TDSE calculations with no field within r_c (full MEP account).

Next, we consider the effect of MEP on PMDs and ATI spectra for CO_2, probed by 800-nm laser pulses containing two and eight optical cycles at a laser intensity of 8.8×10^{13} W/cm^2. The PMDs were produced by projecting the wave packet on Coulomb scattering states in the asymptotic region; see Sec. II. In Figs. 8(a), 8(b), 8(d), and 8(e), we show PMDs for aligned CO_2 at an alignment angle of the maximum TIY, $\beta = 45°$, obtained with and without long-range MEP correction. When we compare the two- and eight-cycle results, we notice the emergence of multiple substructures in the eight-cycle case, which are associated with above-threshold ionization rings, that can be resolved for the longer pulse. From the color bars in Fig. 8, we see that for both two- and eight-cycle pulses, the inclusion of MEP results in the suppression of the ionization yield, however, no clear imprints are found on the fine structure in the PMDs. To capture the quantitative effects of MEP more clearly, we plot ATI spectra for CO_2 at alignment angle $\beta = 45°$ in Figs. 8(c) and 8(f). The ATI intensities were normalized to unity for calculations with and without the MEP effect to ease the comparison. The two-cycle results are summarized in Fig. 8(c), where the dotted line (solid line) denotes the results of TDSE calculations without (with) MEP. The ATI spectrum does not show multiphoton absorption peaks, which is characteristic of ATI spectra for short pulses. Moreover, the figure shows that the inclusion of MEP makes the ATI distribution slightly narrower. Turning to the eight-cycle results in Fig. 8(f), the ATI peaks are now characterized by multiphoton absorption channels. In this case, the inclusion of MEP affects the relative intensity of the ATI peaks, particularly the first couple of peaks at energies of 0.012 and 0.072 a.u., which are affected by the MEP effect. We have produced PMDs and ATI spectra

for CO_2 at an alignment angle of $\beta = 0°$ and reached the same conclusion in that case regarding the effect of the long-range part of the MEP term. We hence face a situation where the long-range part of the MEP, the induced dipole potential, may induce a substantial change in the ionization yields and their alignment dependence, but the shape of the PMDs and ATI spectra only change slightly.

C. Effect of long-range multielectron polarization on alignment-dependent total ionization yields and photoelectron momentum distributions of CS_2

For the CS_2 molecule, the HOMO(xz) and HOMO(yz) were probed by laser pulses containing five optical cycles with a laser peak intensity of 4.5×10^{13} W/cm^2. The alignment-dependent TIYs [incoherent sums of contributions from the HOMO(xz) and HOMO(yz)] are shown in Fig. 9(a), where the dotted line denotes no field within r_c, while the solid line denotes the full MEP treatment; see Sec. II. From Fig. 9(a), we clearly see that MEP has a significant effect on the angular distribution of TIYs: the alignment angle β of maximum TIY shifts from $\beta = 30°$ to $45°$ upon accounting for the long-range MEP term in the TDSE treatment. We notice that the effect of including MEP on the angular distribution of TIYs from CS_2 closely resembles the results for CO_2 in Figs. 3(c) and 3(d). This makes sense since the molecules have the same orbital symmetry and comparable ionization energies. Also, the Keldysh parameter ($\gamma = 1.38$) for CS_2 at a laser intensity of 4.5×10^{13} W/cm^2 is comparable to that for CO_2 at 8.8×10^{13} W/cm^2, where $\gamma = 1.2$, suggesting that these molecules are probed within similar ionization regimes.
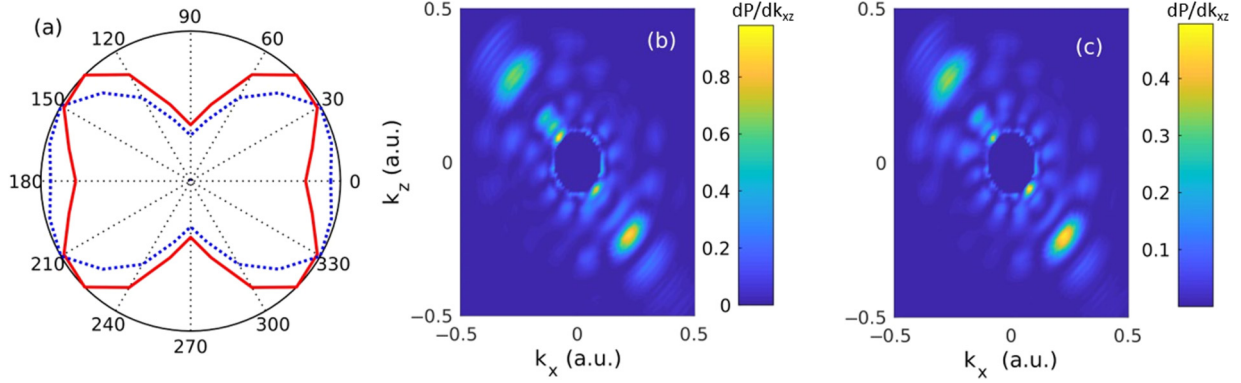
FIG. 9. Effect of MEP on (a) alignment dependence of TIYs for CS_2 obtained as the incoherent sum of the yields from the HOMO(xz) and the HOMO(yz) and (b),(c) photoelectron momentum distributions from the HOMO(xz) of the CS_2 molecule at peak intensity of 4.5×10^{13} W/cm^2 for pulses containing five cycles. In (a), the dotted line denotes no field within r_c, while the solid line denotes full MEP; the TIYs are given on a relative scale. The PMD in (b) refers to TDSE calculations with no field within r_c, while (c) refers to the full MEP account.

Turning to the PMDs of aligned CS_2, the effect of including MEP is highlighted in Figs. 9(b) and 9(c) for aligned CS_2 at alignment angle $\beta = 45°$. In Fig. 9(b), the external field is turned off within r_c, whereas in Fig. 9(c), the full MEP term is accounted for. A qualitative comparison of the two distributions reveals a significant reduction of differential ionization probability for CS_2 upon inclusion of MEP [see the color bars of Figs. 9(b) and 9(c)]; however, no clear observable imprint is found on the fine structure in the PMDs. A detailed analysis of the ATI spectra for CS_2 (not shown here) led to the same conclusions for CS_2 as for the CO_2.

As presented in Table I, the values of the static polarizability components of the CS_2^+ ion are around two or three times larger than those for the CO_2^+ ion. Accordingly, one would expect stronger MEP effects on the angular distribution of TIYs for CS_2 compared with CO_2. The dominant effect of long-range MEP correction is reflected on the TIYs. For example, from comparing the actual TIYs for CO_2 and CS_2 at alignment angle $\beta = 45°$, the TIYs from CO_2 and CS_2 are reduced by 37% and 47%, respectively, upon inclusion of MEP, based on TDSE calculations for pulses containing five optical cycles with peak intensity of 4.5×10^{13} W/cm^2 for CS_2 (5.6×10^{13} W/cm^2 for CO_2). Hence, it can clearly be seen that the effect of MEP is more substantial for CS_2 than for CO_2. The suppression of TIYs for CS_2 and CO_2 is consistent with the size of the anisotropic polarizabilities of their cations.

Now, regarding the impact of MEP on the alignment angle of the maximum TIY, the results presented in Figs. 3 and 9(a) show that the inclusion of long-range MEP shifts the ionization peak from $\beta = 30°$ to $45°$ for both molecules. However, it should be noted that the HOMO orbitals of CS_2 and CO_2 have different structural factors: from analysis of the orbital structural factors for CO_2 and CS_2 reported in Ref. [3], we find significantly different structural factors. In particular, the ratio of $C_{l=4}/C_{l=2}$ is 0.23 for CO_2 vs 0.41 for CS_2. Based on the structural factors for the HOMO orbitals of CO_2 and CS_2, tunneling rates were calculated and the results (not shown) suggest that the differences in orbital structural parameters are also important for the interpretation of the effect of MEP on the angular distribution of TIYs. In brief, the TIY for CS_2

exhibits a peak below an orientation angle of $30°$, whereas the TIY for CO_2 exhibits a peak at $30°$. In this sense, the shift to a peak at $45°$ for both molecules indicates a relatively larger role of MEP in the case of CS_2 than CO_2.

D. Effect of long-range multielectron polarization on alignment-dependent total ionization yields and photoelectron momentum distributions of O_2

The HOMO(xz) and HOMO(yz) of O_2 were probed by laser pulses containing five optical cycles with a laser peak intensity of 8.8×10^{13} W/cm^2. The alignment-dependent TIYs [the summed-up contributions from HOMO(xz) and HOMO(yz) orbitals] are shown in Fig. 10(a), where the dashed line denotes no field within r_c, while the solid line denotes the full MEP treatment; see Sec. II. From Fig. 10(a), we can clearly see that the angular distribution of TIYs has a sharp peak at an alignment angle of $\beta = 45°$ and no significant effect of MEP is observed. This can be due to the fact that the O_2^+ ion has a relatively small polarizability along the laser polarization ($\alpha_{\parallel}$) compared to CO_2 and CS_2; see Table I.

Now we refer to the effect of MEP on the PMDs of O_2. We compare the PMDs at the alignment angle of the maximum TIYs, $\beta = 45°$, in Figs. 10(b) and 10(c). From the color bars, we observe a slight reduction in the differential ionization probability for O_2 upon inclusion of MEP with no clear observable effects on the fine structure in the PMDs. This can be understood since the polarizability of the O_2^+ cation along the laser polarization ($\alpha_{\parallel}$) is relatively small, compared to those for CO_2 and CS_2.

IV. CONCLUSIONS

In this work, we revisited strong-field ionization of aligned O_2, CO_2, and CS_2 molecules. We investigated the effect of accounting for MEP in the TDSE methodology within the SAE approximation on the alignment dependence of TIYs, PMDs, and ATI spectra. Generally, MEP results in two related effects. First, the electrons in the cation polarize and set up a field that counteracts the externally applied field at
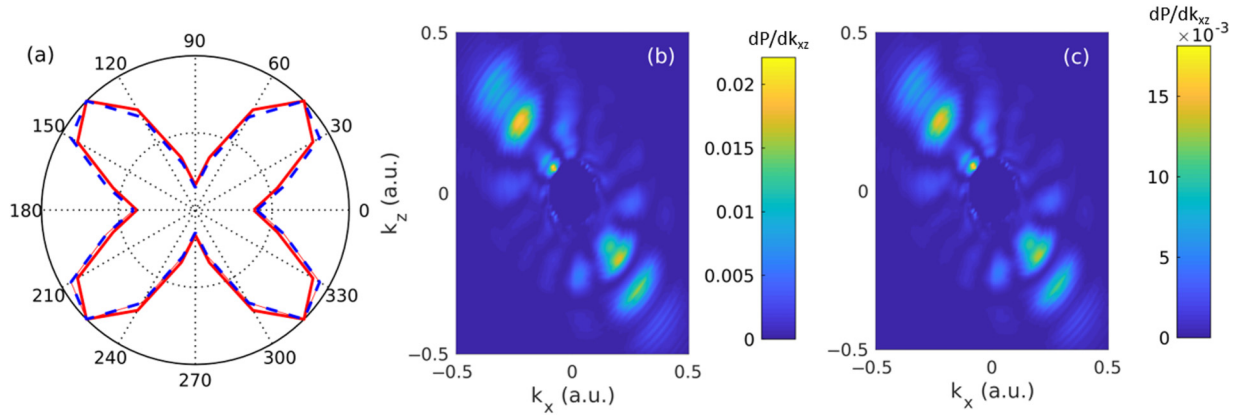
FIG. 10. Effect of MEP on the (a) alignment dependence of TIYs for O_2 obtained as the incoherent sum of the yields from the HOMO(xz) and the HOMO(yz) and (b), (c) photoelectron momentum distributions from the HOMO(xz) of the O_2 molecule at peak intensity of 8.8×10^{13} W/cm^2 for pulses containing five cycles. In (a), the dashed line denotes no field within r_c, while the solid line denotes full MEP, and the TIYs are given on a relative scale. The PMD in (b) refers to TDSE calculations with no field within r_c, while (c) refers to the full MEP account.

short distances. This effect means that the interaction between the single-active electron and the laser field is effectively turned off at distances smaller than $r_c \sim (\alpha_{||})^{\frac{1}{3}}$. Second, the interaction of the time-dependent laser field with the polarizability of the cation results in an induced dipole potential for $r > r_c$. In general, TDSE calculations within the SAE approximation and without the MEP effects suffered from shifting of the population to lower bound states of the potential, as was demonstrated for CO_2. This problem is resolved by turning off the external field within a critical radius r_c. Now, turning to the effect of accounting for long-range MEP, taking this correction term into account improves the calculated angular distributions of TIYs for molecules with large polarizabilities of their cations, i.e., CO_2 and CS_2, in particular at high intensities. For all three considered molecules, the maximum in the TIY is at $\sim 45°$. The calculations show that the long-range part of the induced dipole potential shifts the maximum of the

TIY from $\sim 30°$ to $45°$ for CO_2 and CS_2. For O_2, which has a relatively smaller polarizability, the change to the angular distributions of TIYs induced by the long-range MEP term is negligible. For CO_2 and CS_2, the MEP-induced shift in the maximum of the TIY was rationalized in terms of the alignment- and polarization-dependent changes of the tunneling barrier. In the PMDs and ATI spectra of CO_2 and CS_2, the effect of including long-range MEP is seen as a small change in the width of the distributions and relative intensities of the low-momentum peaks. The present findings are relevant for future investigations of MEP on angular distributions of TIYs and PMDs of oriented molecules.

ACKNOWLEDGMENT

[1] X. M. Tong and C. D. Lin, Empirical formula for static field ionization rates of atoms and molecules by lasers in the barrier-suppression regime, J. Phys. B: At. Mol. Opt. Phys. **38**, 2593 (2005).

[2] H. G. Muller and F. C. Kooiman, Bunching and Focusing of Tunneling Wave Packets in Enhancement of High-Order Above-Threshold Ionization, Phys. Rev. Lett. **81**, 1207 (1998).

[3] M. Abu-samha and L. B. Madsen, Single-active-electron potentials for molecules in intense laser fields, Phys. Rev. A **81**, 033416 (2010).

[4] M. Awasthi and A. Saenz, Breakdown of the single-active-electron approximation for one-photon ionization of the $B^1\Sigma_u^+$ state of H_2 exposed to intense laser fields, Phys. Rev. A **81**, 063406 (2010).

[5] I. Barth, J. Manz, and G. K. Paramonov, Time-dependent extension of Koopmans' picture for ionisation by a laser pulse: Application to H, Mol. Phys. **106**, 467 (2008).

[6] S. Petretti, Y. V. Vanne, A. Saenz, A. Castro, and P. Decleva, Alignment-Dependent Ionization of N_2, O_2, and CO_2 in Intense Laser Fields, Phys. Rev. Lett. **104**, 223001 (2010).

[7] V. P. Majety and A. Scrinzi, Multielectron effects in strong-field ionization of CO_2: Impact on differential photoelectron spectra, Phys. Rev. A **96**, 053421 (2017).

[8] M. Abu-samha and L. B. Madsen, Effect of multielectron polarization in the strong-field ionization of the oriented Co molecule, Phys. Rev. A **101**, 013433 (2020).

[9] M. Abu-samha and L. B. Madsen, Multielectron effects in strong-field ionization of the oriented OCS molecule, Phys. Rev. A **102**, 063111 (2020).

[10] J. Wu, L. Ph. H. Schmidt, M. Kunitski, M. Meckel, S. Voss, H. Sann, H. Kim, T. Jahnke, A. Czasch, and R. Dörner, Multiorbital Tunneling Ionization of the CO Molecule, Phys. Rev. Lett. **108**, 183001 (2012).

[11] V.-H. Hoang, S.-F. Zhao, V.-H. Le, and A.-T. Le, Influence of permanent dipole and dynamic core-electron polarization on tunneling ionization of polar molecules, Phys. Rev. A **95**, 023407 (2017).

[12] H.-P. Kang, S.-P. Xu, Y.-L. Wang, S.-G. Yu, X.-Y. Zhao, X.-L. Hao, X.-Y. Lai, T. Pfeifer, X.-J. Liu, J. Chen, Y. Cheng, and Z.-Z. Xu, Polarization effects in above-threshold ionization

with a mid-infrared strong laser field, J. Phys. B: At. Mol. Opt. Phys. **51**, 105601 (2018).

[13] B. Zhang, J. Yuan, and Z. Zhao, Dynamic Core Polarization in Strong-Field Ionization of CO Molecules, Phys. Rev. Lett. **111**, 163001 (2013).

[14] H. T. Nguyen, Kim-Ngan H. Nguyen, N.-L. Phan, C.-T. Le, D. D. Vu, L.-P. Tran, and V.-H. Le, Imprints of multielectron polarization effects in odd-even harmonic generation from CO molecules, Phys. Rev. A **105**, 023106 (2022).

[15] H. Ohmura, N. Saito, and T. Morishita, Molecular tunneling ionization of the carbonyl sulfide molecule by double-frequency phase-controlled laser fields, Phys. Rev. A **89**, 013405 (2014).

[16] P. Sándor, A. Sissay, F. Mauger, P. M. Abanador, T. T. Gorman, T. D. Scarborough, M. B. Gaarde, K. Lopata, K. J. Schafer, and R. R. Jones, Angle dependence of strong-field single and double ionization of carbonyl sulfide, Phys. Rev. A **98**, 043425 (2018).

[17] J. L Hansen, L. Holmegaard, J. H Nielsen, H. Stapelfeldt, D. Dimitrovski, and L. B. Madsen, Orientation-dependent ionization yields from strong-field ionization of fixed-in-space linear and asymmetric top molecules, J. Phys. B: At. Mol. Opt. Phys. **45**, 015101 (2012).

[18] J. Yu, W. Hu, L. He, C. Wang, S. Luo, and D. Ding, Contribution of resonance excitation on ionization of OCS molecules in strong laser field, J. Phys.: Conf. Ser. **875**, 032030 (2017).

[19] R. Johansen, K. G. Bay, L. Christensen, J. Thøgersen, D. Dimitrovski, L. B. Madsen, and H. Stapelfeldt, Alignment-dependent strong-field ionization yields of carbonyl sulfide molecules induced by mid-infrared laser pulses, J. Phys. B: At. Mol. Opt. Phys. **49**, 205601 (2016).

[20] X. M. Tong, Z. X. Zhao, and C. D. Lin, Theory of molecular tunneling ionization, Phys. Rev. A **66**, 033402 (2002).

[21] L. V. Keldysh, [Sov. Phys. JETP **20**, 1307 (1965)], Zh. Eksp. Teor. Fiz. **47**, 1945 (1964).

[22] F. H. M. Faisal, Multiple absorption of laser photons by atoms, J. Phys. B: At. Mol. Phys. **6**, L89 (1973).

[23] H. R. Reiss, Effect of an intense electromagnetic field on a weakly bound system, Phys. Rev. A **22**, 1786 (1980).

[24] D. Dimitrovski, C. P. J. Martiny, and L. B. Madsen, Strong-field ionization of polar molecules: Stark-shift-corrected strong-field approximation, Phys. Rev. A **82**, 053404 (2010).

[25] L. Holmegaard, J. L. Hansen, L. Kalhøj, S. L. Kragh, H. Stapelfeldt, F. Filsinger, J. Küpper, G. Meijer, D. Dimitrovski, M. Abu-samha, C. P. J. Martiny, and L. B. Madsen, Photoelectron angular distributions from strong-field ionization of oriented molecules, Nat. Phys. **6**, 428 (2010).

[26] O. I. Tolstikhin, T. Morishita, and L. B. Madsen, Theory of tunneling ionization of molecules: Weak-field asymptotics including dipole effects, Phys. Rev. A **84**, 053423 (2011).

[27] L. B. Madsen, F. Jensen, O. I. Tolstikhin, and T. Morishita, Structure factors for tunneling ionization rates of molecules, Phys. Rev. A **87**, 013406 (2013).

[28] D. Dimitrovski, M. Abu-samha, L. B. Madsen, F. Filsinger, G. Meijer, J. Küpper, L. Holmegaard, L. Kalhøj, J. H. Nielsen, and H. Stapelfeldt, Ionization of oriented carbonyl sulfide molecules by intense circularly polarized laser pulses, Phys. Rev. A **83**, 023405 (2011).

[29] D. Pavičić, K. F. Lee, D. M. Rayner, P. B. Corkum, and D. M. Villeneuve, Direct Measurement of the Angular Dependence of Ionization for N$_2$, O$_2$, and CO$_2$ in Intense Laser Fields, Phys. Rev. Lett. **98**, 243001 (2007).

[30] V. Kumarappan, L. Holmegaard, C. Martiny, C. B. Madsen, T. K. Kjeldsen, S. S. Viftrup, L. B. Madsen, and H. Stapelfeldt, Multiphoton Electron Angular Distributions from Laser-Aligned CS$_2$ Molecules, Phys. Rev. Lett. **100**, 093006 (2008).

[31] M. Abu-samha and L. B. Madsen, Theory of strong-field ionization of aligned CO$_2$, Phys. Rev. A **80**, 023401 (2009).

[32] M. W. Schmidt, K. K. Baldridge, J. A. Boatz, S. T. Elbert, M. S. Gordon, J. H. Jensen, S. Koseki, N. Matsunaga, K. A. Nguyen, S. Su, T. L. Windus, M. Dupuis, and J. A. Montgomery Jr, General atomic and molecular electronic structure system, J. Comput. Chem. **14**, 1347 (1993).

[33] T. K. Kjeldsen, L. A. A. Nikolopoulos, and L. B. Madsen, Solving the m-mixing problem for the three-dimensional time-dependent Schrödinger equation by rotations: Application to strong-field ionization of H$_2{}^+$, Phys. Rev. A **75**, 063427 (2007).

[34] M. R. Hermann and J. A. Fleck, Split-operator spectral method for solving the time-dependent schrödinger equation in spherical coordinates, Phys. Rev. A **38**, 6000 (1988).

[35] T. Brabec, M. Côté, P. Boulanger, and L. Ramunno, Theory of Tunnel Ionization in Complex Systems, Phys. Rev. Lett. **95**, 073001 (2005).

[36] Z. Zhao and T. Brabec, Tunnel ionization in complex systems, J. Mod. Opt. **54**, 981 (2007).

[37] R. D. Johnson III, editor, NIST computational chemistry comparison and benchmark database, release 21, Aug. 2020, edited by NIST Standard Reference Database No. 101.

[38] M. Abu-samha and L. B. Madsen, Photoelectron angular distributions from polar molecules probed by intense femtosecond lasers, Phys. Rev. A **82**, 043413 (2010).

[39] M. Abu-samha and L. B. Madsen, Alignment dependence of photoelectron momentum distributions of atomic and molecular targets probed by few-cycle circularly polarized laser pulses, Phys. Rev. A **94**, 023414 (2016).

[40] N. I. Shvetsov-Shilovski, D. Dimitrovski, and L. B. Madsen, Ionization in elliptically polarized pulses: Multielectron polarization effects and asymmetry of photoelectron momentum distributions, Phys. Rev. A **85**, 023428 (2012).